Heterotrimeric G proteins precouple with G protein-coupled receptors in living cells

Muriel Nobles, Amy Benians, and Andrew Tinker*

British Heart Foundation Laboratories and Department of Medicine, University College London, 5 University Street, London WC1E 6JJ, United Kingdom

Edited by Lily Y. Jan, University of California, San Francisco, CA, and approved October 26, 2005 (received for review June 9, 2005)

Using fluorescence resonance energy transfer (FRET) microscopy, we investigate how heterotrimeric G proteins interact with G protein-coupled receptors (GPCRs). In the absence of receptor activation, the α2A adrenergic and muscarinic M4 receptors are present on the cell membrane as dimers. Furthermore, there is an interaction between the G protein subunits αo, $\beta 1$, and $\gamma 2$ and a number of GPCRs including M4, α2A, the adenosine A1 receptor, and the dopamine D2 receptor under resting conditions. The interaction between GPCRs and Gα proteins shows specificity: there is interaction between the α2A receptor and Go, but little interaction between the α2A receptor and Gs. In contrast, the predominantly Gs-coupled prostacyclin receptor interacted with Gs, but there was little interaction between the prostacyclin receptor and Go. Inverse agonists did not change the FRET ratio, whereas the addition of agonist resulted in a modest fall. Our work suggests that GPCR dimers and the G protein heterotrimer are present at the cell membrane in the resting state in a pentameric complex.

Two opposing ideas are invoked to explain how membrane bound signaling proteins transfer information after activation. In the first, components in the membrane freely diffuse and interactions occur through "collision coupling" determined by diffusion. Historically, such mechanisms are thought to govern the interaction of G protein-coupled receptor (GPCR) with G protein and the interaction of G protein with downstream enzymes and ion channels. Signal amplification is a key feature of this mechanism (1–3). A second mechanism is the "physical scaffolding" hypothesis in which component proteins interact directly or indirectly with each other. The best example of this is the role of InaD in the *Drosophila* photoreceptor that scaffolds via PDZ domains the light-sensing GPCR rhodopsin, Ca^{2+} influx TRP channels, phospholipase C, and protein kinase C (4). In principle, this is a way of generating fast activation, fast signal termination, and specificity. A variant of this hypothesis is the localization of proteins in membrane signaling microdomains such as caveolae and lipid rafts.

The G protein-gated K^+ channel (GIRK) was first identified in atrial myocytes. Channel activation occurs after binding of acetylcholine to muscarinic M2 receptors (5) and is responsible for slowing of the heart rate in response to vagal stimulation (6, 7). Analogous GIRK currents are present in neurons and neuroendocrine cells (8). Activation of native and cloned GIRK channels has been shown to involve a direct, membrane-delimited interaction with the G$\beta\gamma$ subunit (9, 10). One critical point is that the activation occurs rapidly in both native and heterologous settings: complete channel activation can occur within 1 s of the addition of agonist (11–13). Such fast rates of signaling suggest that the components diffuse only small distances, if at all. From these considerations alone it is an appealing hypothesis to propose that the components may be physically scaffolded together. Our own studies and those of others suggest that the Gi/o heterotrimer is associated with the GIRK channel, and this confers fast, selective receptor-mediated activation (14–17). In this study, we consider upstream events and examine the interaction of GPCRs with heterotrimeric G proteins. There is an emerging consensus that suggests that GPCRs function as dimers or even higher-order oligomers (18–20). Potentially, this would allow one GPCR subunit in the dimer to contact the Gα subunit and the other to contact the G$\beta\gamma$ subunit. However, it is still under debate whether the receptor dimer contacts the G protein before agonist exposure. There has been biochemical data hinting at this, but it is not clear whether this is a general feature of GPCR–G protein interactions (21–25). More recently, bioluminescence resonance energy transfer studies on suspensions of cells have suggested some basal interaction between components of the G protein heterotrimer and the GPCR; however, this was solely attributed to constitutive activity of some of the receptor constructs (26). Furthermore, biochemical studies have proposed a pentameric complex between a receptor dimer and the G protein heterotrimer (27). Such "precoupling" of GPCR dimer and G protein heterotrimer would lead to fast effector activation specifically for example GIRK channels and may ensure signaling fidelity. In this study, we test this hypothesis in living cells.

Materials and Methods

Molecular Biology, Cell Culture, and Transfection. Fluorescent G protein subunits were used as described (13, 28, 29). An identical strategy was adopted to fuse yellow fluorescent protein (YFP) to Go to generate a functional G protein α subunit i.e., the subunit is targeted to the membrane by an N-terminal dual palmitoylation sequence from GAP43 (29). A PCR-based approach was used to clone receptor cDNAs in frame into pECFP-N1 and pEYFP-N1 (Clontech) using KpnI and HindIII as the cloning sites. All constructs were sequenced to confirm their identity. Cell culture, transient transfection, and generation of HEK-293 stable cell lines have been described (14, 15). Experiments were performed 2–3 days after transfection. In electrophysiological experiments, transfected cells were identified by epifluorescence after transfection of the intrinsically fluorescent species.

Electrophysiology. Patch clamping was carried out as described (12, 30). Cell capacitance was ≈15 pF, and series resistance (<10 MΩ) was at least 75% compensated by using the amplifier. Cells were perfused by using a gravity-fed bath perfusion system. Drugs were applied via a fast agonist application system. Pipette solution (107 mM KCl/1.2 mM $MgCl_2$/5 mM Hepes/2 mM MgATP/0.3 mM Na_2GTP; KOH to pH 7.2, ≈140 mM total K^+) and bath solution (140 mM KCl/2.6 mM $CaCl_2$/1.2 mM $MgCl_2$/5 mM Hepes, pH 7.4) were used. The chemicals were from Sigma or Calbiochem; drugs were made up as concentrated stocks solutions and kept at −20°C.

Microscopy. Cells for imaging were subcultured onto 25-mm glass coverslips and then placed into a watertight cell imaging chamber at room temperature, or were subcultured onto 35-mm culture dishes with integral no. 0 glass coverslip bottoms (Mattek).

Confocal Microscopy. Before imaging, cells were overlaid with Hepes buffered OPTI-MEM without phenol red (Invitrogen). HEK293

Conflict of interest statement: No conflicts declared.

This paper was submitted directly (Track II) to the PNAS office.

Abbreviations: GPCR, G protein-coupled receptor; GIRK, G protein-gated K^+ channel; PTx, pertussis toxin; CFP, cyan fluorescent protein.

*To whom correspondence should be addressed. E-mail: a.tinker@ucl.ac.uk.

www.pnas.org/cgi/doi/10.1073/pnas.0504778102

cells were imaged by using a BioRad Radiance 2100 confocal microscope with a ×60 Nikon Plan Apo oil objective (1.40 numerical aperture). Cyan fluorescent protein was excited with a 457-nm laser line, and images were obtained by using a 470- to 500-nm band pass filter. Yellow fluorescent protein was excited with a 514-nm laser line, and emission was measured between 530 and 570 nm. The FRET imaging conditions were obtained with excitation using a 457-nm laser line, and emission measured between 530 and 570 nm. Multiple images were acquired sequentially. Intensities in the CFP, YFP, and FRET set of imaging conditions were determined from membrane-delimited regions of interest drawn by hand at high magnification using LASERPIX software. The background-subtracted intensities were analyzed to determine FRET ratios using three-cube protocols (see below). Sixteen-bit images were obtained with identical laser powers, photomultiplier gain, and pinhole size and were optimized to examine cells with moderate expression of both constructs. Care was taken to avoid saturating images. Agonist and inverse agonists were directly added to the dish.

Digital Fluorescence Microscopy. We also used a standard fluorescent microscope (Nikon TE200 ×60 Plan Apo oil objective 1.40 numerical aperture), equipped with a back illuminated digital charge-coupled device (CCD) camera (Roper Scientific MicroMax 1024 EB) and high-speed CCD detector control, to measure FRET ratios. Samples were excited by using a mercury lamp with an excitation filter wheel, and emission filters were selected through an emission filter wheel (Sutter Instruments, Lambda-10/2). The following filter sets were used (excitation, emission): YFP (500 ± 10 nm, 535 ± 15 nm), CFP (430 ± 12.5 nm, 465 ± 20 nm), FRET (430 ± 12.5 nm, 535 ± 15 nm). Sixteen-bit images were acquired and analyzed with METAMORPH software (version 6.1, Universal Imaging). Background values used were regions containing no cells in the viewing field. Three-cube parameters and FRET ratio were calculated as above from membrane-delimited regions of interest. It is worth noting that, on both microscopy systems, the SEM of the FRET ratio was generally <5% of the mean, and this compares favorably with other methods (31).

The FRET ratio (FR) measures the fractional increase in YFP emission due to FRET and was calculated according to the following equation (32):

$$FR = [S_{FRET}(DA) - R_{D1} \times S_{CFP}(DA)]/R_{A1} \times [S_{YFP}(DA) - R_{D2} \times S_{CFP}(DA)]. \quad [1]$$

S_{CUBE} (SPECIMEN) denotes an intensity measurement, where CUBE indicates the filter cube (CFP, YFP, or FRET) and SPECIMEN indicates whether the cell is expressing donor (D; CFP), acceptor (A; YFP) or both (DA). $R_{D1} = S_{FRET}(D)/S_{CFP}(D)$, $R_{D2} = S_{YFP}(D)/S_{CFP}(D)$, and $R_{A1} = S_{FRET}(A)/S_{YFP}(A)$ are predetermined constants from measurements applied to single cells expressing only CFP- or YFP-tagged molecules. "net FRET" images are displayed in a number of places and were calculated according to $S_{FRET}(DA) - R_{D1} \times S_{CFP}(DA) - R_{A1} \times [S_{YFP}(DA) - R_{D2} \times S_{CFP}(DA)]$. If the FRET ratio = 1 (i.e., no FRET) then the above equation will equal zero. Any excess signal (i.e., FRET ratio >1) will manifest as increased intensity above background. It is possible to manipulate images on a pixel-by-pixel basis and thus obtain spatial information on the FRET signal. Images were pseudocolored, filtered, and converted to 24-bit RGB files for display (TIFF or JPEG).

Results

In this study, we use a laser scanning confocal microscope and a digital fluorescence microscope as described to perform FRET microscopy (13, 33). FRET is a process by which a fluorophore (donor, i.e., CFP) in an excited state may transfer its excitation energy to a neighboring fluorophore (acceptor, i.e., YFP) through a dipole–dipole interaction. The emission spectra of the donor fluorophore must overlap with the excitation spectra of the acceptor. It is a strongly distance- and orientation-dependent phenomenon; generally, acceptor and donor have to be within 50–100 Å. Practically, it can be measured in a number of ways including donor dequenching, donor lifetime measurements, or sensitized acceptor emission. FRET is increasingly used to monitor protein–protein interactions in living cells. We quantify the FRET signal by calculating excess acceptor emission using three-cube FRET ratios from regions of interest defined on the relevant cellular compart-

Table 1. Values for FRET ratios under various conditions

Constructs	FRET ratio	
	Confocal	CCD
CFP+YFP*	0.94 ± 0.03 (n = 36)	0.97 ± 0.03 (n = 34)
α2A-CFP+KCNQ1-YFP	0.90 ± 0.04 (n = 19)	0.90 ± 0.02 (n = 24)
D2-CFP+M4-YFP*	0.94 ± 0.05 (n = 14)	ND
α2A-CFP+α2A-YFP	1.54 ± 0.06 (n = 34, P < 0.001)	1.72 ± 0.06 (n = 29, P < 0.001)
M4-CFP+M4-YFP	1.88 ± 0.15 (n = 6, P < 0.001)	2.02 ± 0.12 (n = 12, P < 0.001)
Go-CFP+α2A-YFP	1.72 ± 0.07 (n = 28, P < 0.001)	ND
Go-CFP+α2A-YFP+Gβ1+Gγ2	1.41 ± 0.07 (n = 13, P < 0.01)	1.66 ± 0.12 (n = 11, P < 0.001)
Gs-CFP+α2A-YFP	1.18 ± 0.03 (n = 13, NS)	ND
Gs-CFP+α2A-YFP+Gβ1+Gγ2	ND	1.06 ± 0.05 (n = 19, NS)
α2A-CFP+Gβ1-YFP+Gγ2+Go	1.54 ± 0.08 (n = 19, P < 0.001)	1.90 ± 0.09 (n = 22, P < 0.001)
α2A-YFP+Gβ1+Gγ2-CFP+Go	ND	1.69 ± 0.12 (n = 6, P < 0.001)
Go-CFP+M4-YFP	2.08 ± 0.17 (n = 11, P < 0.001)	ND
M4-CFP+Gβ1-YFP+Gγ2+Go	1.66 ± 0.07 (n = 12, P < 0.001)	1.51 ± 0.05 (n = 18, P < 0.001)
M4-YFP+Gβ1+Gγ2-CFP+Go	ND	1.84 ± 0.20 (n = 8, P < 0.001)
Go-CFP+A1-YFP	1.59 ± 0.09 (n = 19, P < 0.001)	ND
A1-CFP+Gβ1-YFP+Gγ2+Go	1.48 ± 0.10 (n = 13, P < 0.001)	1.50 ± 0.05 (n = 18, P < 0.001)
A1-YFP+Gβ1+Gγ2-CFP+Go	1.67 ± 0.17 (N = 6, P < 0.001)	1.53 ± 0.09 (n = 12, P < 0.001)
D2S-YFP+Go-CFP	1.55 ± 0.08 (N = 16, P < 0.001)	ND
D2S-YFP+Go-CFP+Gβ1+Gγ2	ND	1.40 ± 0.09 (n = 12, P < 0.01)
IP-YFP+Go-CFP+Gβ1+Gγ2	1.22 ± 0.09 (N = 16, NS)	ND
IP-YFP+Gs-CFP+Gβ1+Gγ2	1.96 ± 0.14 (N = 13, P < 0.001)	1.76 ± 0.09 (n = 20, P < 0.001)

Statistical significance was calculated by using one-way ANOVA with a Bonferroni post hoc test using α2A-CFP+KCNQ1-YFP as the control conditions. The data shown for CFP+YFP and D2-CFP+M4-YFP (also indicated by *) is taken from Benians *et al.* (13).

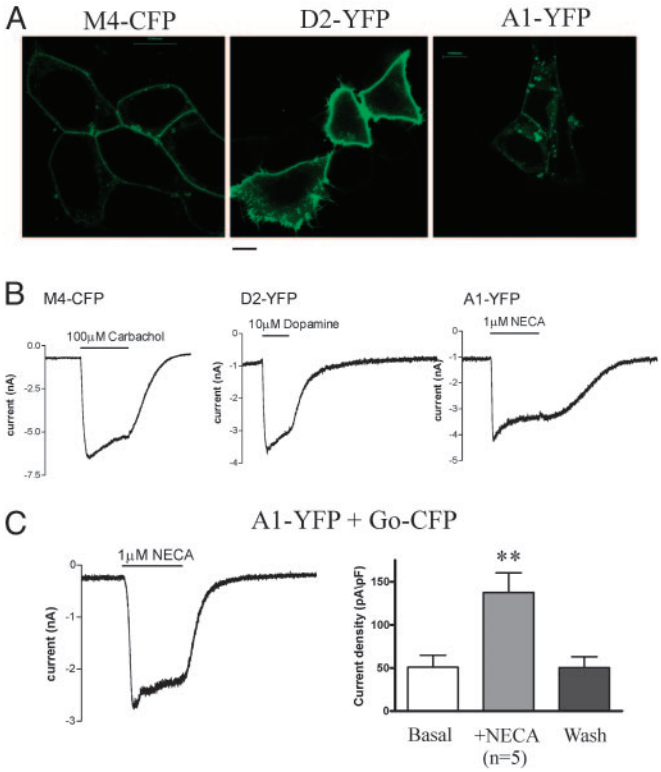

Fig. 1. Tagging of different GPCRs led to expression at the plasma membrane and maintains their functional coupling to GIRK channels. (*A*) Representative confocal images showing that expression of tagged GPCRs as indicated. (Scale bar, 10 μm.) (*B*) Functional coupling of M4, D2, and A1 to GIRK channels in HEK293 cells. Transient transfection of the CFP and YFP constructs into a HEK-293 cell line stably expressing Kir3.1/3.2A. Membrane currents are studied under voltage clamp conditions at a holding potential of −60 mV. The application of relevant agonist elicited inward K^+ currents. (*C*) Expression of Go-CFP and A1-YFP in HEK293 cells stably expressing Kir3.1 and Kir3.2A rescues coupling between the receptor and channel. Cells were PTx treated (100 ng/ml for 16 h) to inactivate all endogenous Gi/o G proteins; **, $P < 0.01$.

ment, i.e., the plasma membrane. We have previously performed a number of controls. Firstly, we optimized microscopy conditions to examine an ≈1:1 molar expression ratio of CFP and YFP constructs by using a CFP–YFP dimeric fusion construct. Secondly, we have established that (*i*) coexpression of CFP and YFP and (*ii*) coexpression of two membrane-localized GPCRs (D2-CFP and M4-YFP), which are not thought to form heterodimers, did not show FRET (13, 33). In this study, we also perform another control in which we coexpress a completely unrelated membrane protein (KCNQ1 K^+ channel) together with a GPCR at similar levels of expression (α2A-CFP plus KCNQ1-YFP) and show that no FRET occurs between these constructs. We use this as a control for statistical comparisons with other potentially interacting proteins, as shown in Table 1.

The α2A-adrenergic and the M4 muscarinic receptors couple to the inhibitory, pertussis toxin (PTx)-sensitive subfamily of G proteins (Gi/o). We first examined whether these receptors can exist as homodimers on the cell membrane by using FRET microscopy. Using standard DNA cloning techniques, the cytoplasmic C termini of the two receptors were fused in frame with the CFP and YFP. Fluorescently tagged α2A and M4 are both expressed at the cell membrane, with little intracellular retention (Figs. 1 and 2). These constructs were expressed in a stable cell line expressing the GIRK channel subunits, Kir3.1 and 3.2A, and we examined agonist-induced activation of the currents using whole-cell patch-clamping. Such experiments revealed these constructs to be functional (Fig. 1*B* and data not shown). In addition, we examined whether a fluorescent receptor (A1-YFP) was able to couple to a fluorescent PTx resistant G protein (Go-CFP) (29). Fig. 1*C* shows that expression of Go-CFP was able to rescue coupling in PTx treated cells between the receptor and GIRK channel.

We then coexpressed the CFP- and YFP-tagged receptor constructs together in HEK293 cells. A clear FRET signal was observed on the cell membrane for both receptors, and three-cube quantification revealed this to be significant (Fig. 2 and Table 1). These results show that both the α2A and M4 receptors potentially form homodimers or higher-order homooligomers on the cell membrane.

We next examined for possible interaction between GPCRs and G protein subunits. In addition to the α2A and M4 receptors, we also fused the C termini of the A1 adenosine receptor and D2S dopamine receptor (D2) with CFP and YFP. Once again, these receptors show prominent expression on the cell membrane and are functional (Fig. 1 and data not shown). In addition, we fused YFP with the Go α subunit (Go) using our previously published approach and combined this with a mutation to render it resistant to PTx (29). The construct is membrane localized, and the patch-clamp technique revealed the construct to be functional. Go-YFP was expressed in HEK293 cells expressing Kir3.1/3.2A, and the A1 receptor and the cells were treated with 100 ng/ml PTx overnight. Expression of the Go-YFP construct was able to rescue coupling between the A1 receptor and the GIRK channel (data not shown).

We then examined for evidence of FRET between the receptors and G protein subunits namely (Go-CFP, Go-YFP, Gβ1-YFP, and Gγ2-CFP). In Fig. 3, we show some representative images obtained with both laser scanning confocal microscopy and digital fluorescence microscopy. The FRET ratios are summarized in Table 1. Using both systems, there is a significant FRET signal between all of the GPCRs studied and the Go α subunit, β1, and γ2 G protein subunits. In contrast, the control proteins, α2A-CFP and KCNQ1-YFP, did not show FRET. Generally we have found that there is sufficient free G$\beta\gamma$ in HEK293 cells to complex with heterologously expressed G protein α subunits to fully reconstitute signaling (15, 29). However, we also examined conditions in which we overexpressed Gβ1 and Gγ2 with Go-CFP, and similar results were obtained. In contrast, overexpression of Gβ1-YFP and Gγ2-CFP without the other components of the G protein heterotrimer led to intracellular retention and failure of the fluorescent construct to translocate to the plasma membrane (Fig. 4*A*). Therefore, it was necessary to coexpress the Go α, Gβ1, and/or Gγ2 subunits to achieve good membrane localization in keeping with the findings of other investigators (34).

Our methodology for examining FRET relies on the quantitation of sensitized acceptor emission. We also examined whether we could observe FRET by measuring donor dequenching after acceptor photobleaching. We optimized microscopy conditions to obtain 70–90% acceptor photobleaching after exposure to high power of the 514-nm laser line with minimal concomitant CFP bleaching (≈7–10%). CFP fluorescence increased by 11 ± 2% ($n = 18, P < 0.001$) for α2A-CFP plus α2A-YFP, 12 ± 3% ($n = 14$, $P < 0.001$) for Go-CFP plus α2A-YFP, 10 ± 3% ($n = 10, P < 0.01$) for Go-CFP plus M4-YFP, and 15 ± 3% ($n = 9$, $P < 0.01$) for Go-CFP plus D2-YFP. A sample experiment is shown in Fig. 4*B*.

We next looked at the specificity of these interactions between GPCRs and Gα subunits. Initially, we compared the interaction between the Gi/o-coupled α2A receptor and Go-CFP and Gs-CFP. In both microscopy systems, we saw pronounced FRET with Go but little or none with Gs (Fig. 5 and Table 1). Furthermore, we examined the interaction between a predominantly Gs-coupled receptor, namely the prostacyclin receptor (IP), and Gs and compared this to Go. We observed significantly higher FRET between the prostacyclin receptor and Gs than with Go, indicating that this interaction likely plays an important role in receptor coupling and further suggests the existence of specific signaling complexes. These

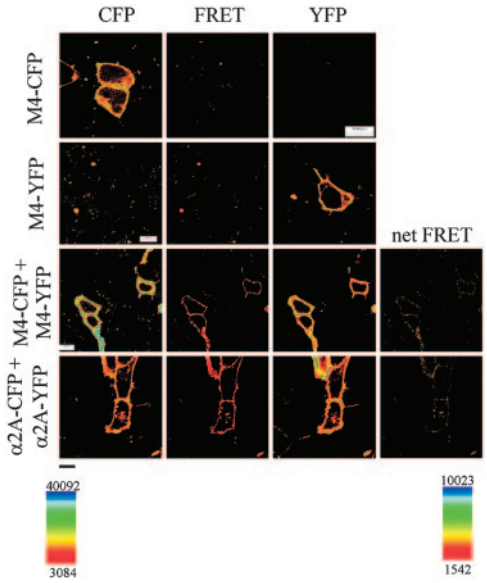

Fig. 2. Oligomerization of a2A and M4 receptors on the plasma membrane. Representative confocal images were collected of HEK293 cells expressing M4-CFP, M4-YFP, M4-CFP together with M4-YFP, as well as α2A-CFP together with α2A-YFP. These images were obtained with a laser-scanning confocal microscopy as described in *Materials and Methods*. Three-cube net FRET signal, shown for the cells coexpressing M4-CFP with M4-YFP and α2A-CFP with α2A-YFP, is delimited to the plasma membrane. (Scale bar, 10 μm.)

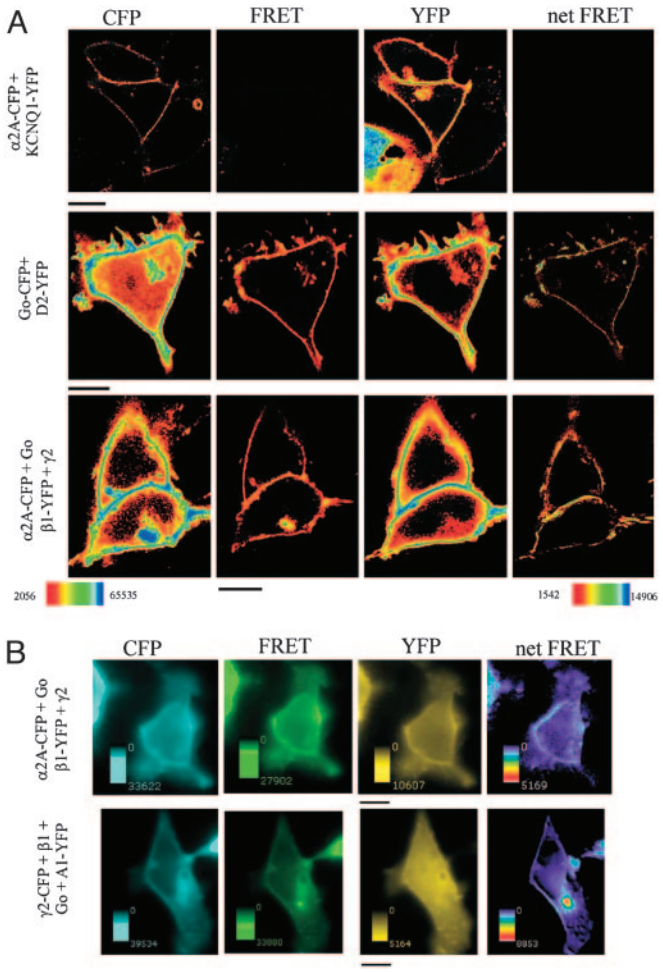

Fig. 3. Receptor precoupling with heterotrimeric G protein subunits. (*A*) Confocal images of HEKs cotransfected with the indicated plasmids. (*Right*) The three-cube net FRET images. (Scale bar, 10 μm.) (*B*) Images obtained with a back illuminated CCD camera (see *Materials and Methods*). (*Right*) Images showing the three-cube net FRET signal obtained with the three-cube FRET module (METAMORPH, Universal Imaging). (Scale bar, 10 μm.)

results suggest specific interactions between GPCRs and Gα subunits. To further test the validity of these FRET measurements, we tried to exclude the possibility that FRET had arisen from random collision of fluorescent species in the membrane (35–37). We plotted the FRET ratio against donor intensity per pixel, which is equivalent to the concentration. Three-cube measurements show a tendency for increased FRET ratios at higher donor concentration (37). The FRET ratio was significantly higher however for α2A-YFP and Go-CFP compared to α2A-YFP and Gs-CFP expressed at comparable levels (Fig. 6*A*). The three-cube FRET ratio was not correlated with expression levels (donor added to acceptor intensity per pixel, Fig. 6*B*), but was most strongly correlated with the donor to acceptor ratio, and this observation is discussed below (Fig. 6*C*).

We next performed some studies to examine the effects of the addition of inverse agonists and agonists. The specific FRET signal between Gi/o-coupled receptors and Go could arise because of constitutive activity of the receptor constructs. Thus, we used rauwolscine and 1,3-dipropyl-8-cyclopentylxanthine (DPCPX) as inverse agonists at the adrenergic α2A and adenosine A1 receptors, respectively (38, 39). In cells expressing Go-CFP plus α2A-YFP and Go-CFP plus A1-YFP and imaged by using confocal microscopy, the FRET ratio did not significantly change on the addition of the inverse agonist (Go-CFP plus α2A-YFP in paired cells, $n = 20$, FRET ratio = 2.03 ± 0.10; and plus 1 μM rauwolscine = 1.96 ± 0.17, not significant, paired *t* test; Go-CFP plus A1-YFP in paired cells, $n = 8$, FRET ratio = 1.83 ± 0.11, and plus 1 μM DPCPX = 1.74 ± 0.17, not significant, paired *t* test). In contrast, the addition of agonist did lead to a significant albeit modest change. In PTx-treated cells expressing Go-CFP plus α2A-YFP and imaged by using confocal microscopy the FRET ratio significantly decreases on the addition of agonist (in paired cells, $n = 9$, FRET ratio = 1.76 ± 0.16, and plus 3 μM norepinephrine = 1.63 ± 0.14, $P = 0.025$, paired *t* test). The mean fall in FRET ratio is calculated as ≈20%.

Discussion

Our data support the existence of a specific pentameric complex in living intact cells between homodimeric GPCRs and the heterotrimeric G protein. This is shown to be a general phenomenon that is found to some extent with all of the Gi/o-coupled receptors tested and also with the Gs-coupled prostacyclin receptor. In addition, the interaction is selective for the G protein family that the receptor is thought to couple to in its native environment in cell signaling.

It is becoming increasingly clear that GPCRs can assemble as dimers or higher-order oligomers (18–20). This feature has been described for a number of receptor families, but not specifically for the α2A adrenergic receptor and M4 muscarinic receptor. In this study, we show FRET between CFP and YFP tagged GPCRs compatible with homooligomerization. Is there any possible reason for why the vast majority, if not all, serpentine receptors should function in this fashion? Structural studies of the receptor and G protein interface have led to proposals on potential points of contact between the heterotrimeric G protein and the receptor (40). The cytosolic surface of a single receptor monomer is too small to accommodate all these points of contact with the G protein simultaneously, and it has been proposed (40) that two receptor molecules might be necessary to allow the binding of the G protein heterotrimer.

Our FRET studies suggest a stable interaction between a variety of Gi/o-coupled receptors (α2A, M4, D2S, and A1) with the G

PHARMACOLOGY

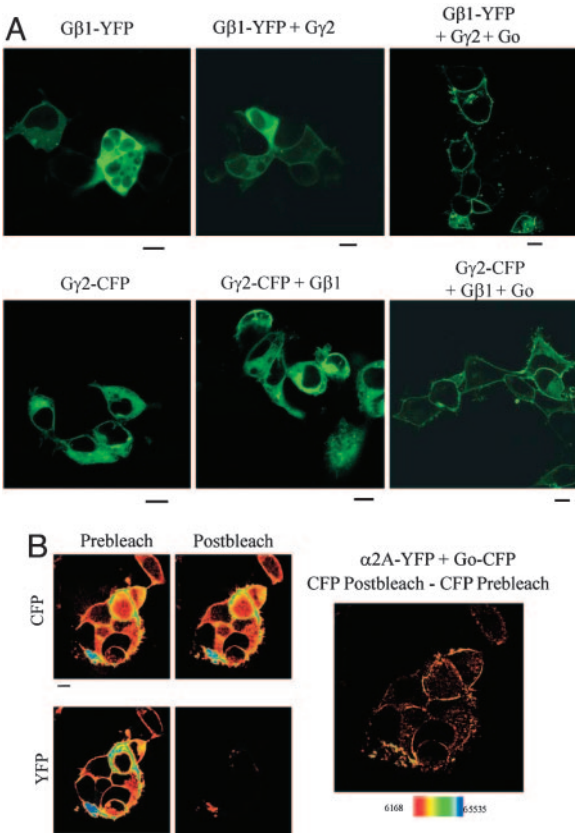

Fig. 4. Role of Goα in the translocation of G protein subunits and in the precoupling with the GPCR. (*A*) Confocal images showing the intracellular distribution of Gβ1-YFP and Gγ2-CFP when expressed in HEK293 cells. (*Right*) The coexpression of Goα together with Gγ2 or Gβ1 led to translocation of the Gβ1-YFP (*Upper*) and Gγ2-CFP (*Lower*), respectively, to the plasma membrane. Under other expression conditions, there was significant intracellular retention. (*B*) Acceptor (i.e., α2A-YFP) photobleaching was carried out by using the 514-nm laser line. The subtracted image of CFP postbleach − CFP prebleach shows an increase of the donor fluorescence (i.e., Go-CFP) after acceptor photobleaching. (Scale bar, 10 μm.)

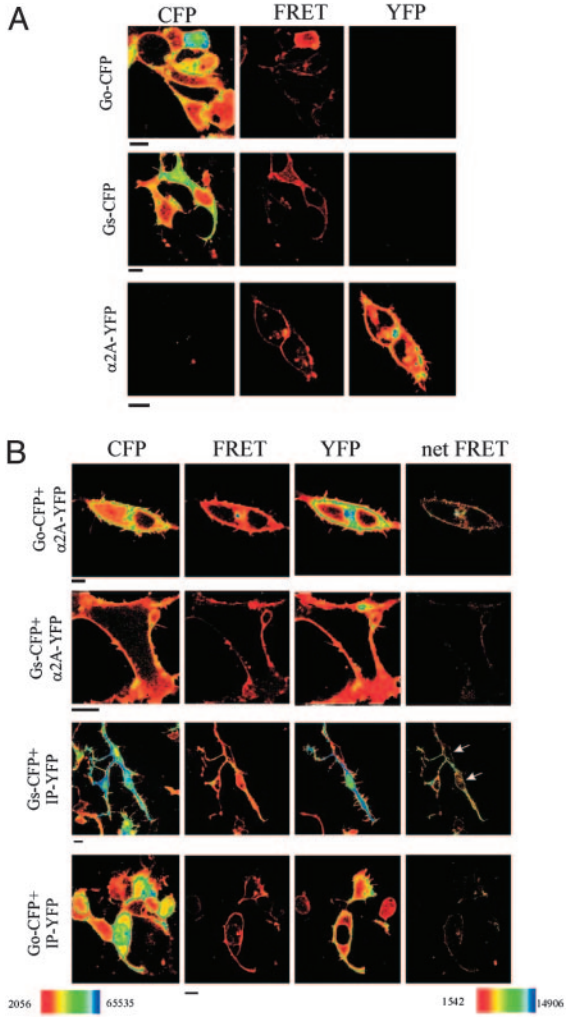

Fig. 5. Receptor precoupling: specificity of the interaction between GPCRs and Gα. (*A*) Confocal images showing the cellular distribution of Go-CFP, Gs-CFP, and α2A-YFP in HEKs cells. (*B*) The specificity of the interaction between α2A-YFP and Goα-CFP as well as between IP-YFP (prostacyclin receptor) and Gs-CFP. Parts of the image IP-YFP and Gs-CFP are saturating and arrows indicate regions of interest which are not and have membrane delimited FRET. For all images, cells were transfected with the plasmids as indicated. (Scale bar, 10 μm.)

protein Go and the Gs-coupled prostacyclin receptor with Gs. The interaction shows selectivity because Gs does not precouple with the Gi/o-coupled receptors and the predominantly Gs-coupled IP receptor does precouple with Gi/o. In addition, we demonstrate interaction of some of these receptors with Gβ1 and Gγ2 under resting conditions. This result provides strong support for receptor precoupling to the heterotrimeric G protein. In the classical "collision-coupling" models of the G protein cycle, receptor–G protein interaction is determined by the diffusive properties of the two proteins. Only on collision with the G protein is the agonist-occupied receptor able to catalyze GDP release, and subsequent GTP binding stabilizes the active conformation of the G protein. The receptor and G protein heterotrimer then dissociate, and the active signaling species interact by diffusion with effectors. The receptor is released to act catalytically and interact with other G protein heterotrimers. In most signaling cascades, it is clear that G proteins are present in 10–100 molar excess compared to receptors. Thus, in a S49 cell, there are ≈1,000 β-adrenergic receptors, 100,000 molecules of Gs, and ≈4,000 molecules of adenylate cyclase (41), and a single receptor can potentially activate up to 100 Gs molecules (42). Such mechanisms are supported by classic work on visual transduction in rods via the rhodopsin–transducin system and cAMP signaling in turkey erythrocytes (1, 43). However, a number of observations are not consistent with this hypothesis. It is clear that a G protein heterotrimer can form a stable biochemical complex with the receptor that is preserved after the addition of agonist (21, 25). In a biochemical tour-de-force, Baneres and Parello (27) demonstrated *in vitro* that the leukotriene B4 dimeric receptor and the G protein heterotrimer form a pentameric assembly (27). Secondly, in radioligand binding studies, addition or expression of the G protein heterotrimer endows a significant fraction of the receptor population with high agonist affinity (44, 45) and it is also possible to immunoprecipitate complexes of receptor and G protein (21–24, 46).

Current models of GPCR activation, such as the cubic ternary complex model, include states in which the G protein forms a complex with the inactive GPCR (47). Other investigators have detected some basal interaction between the G protein heterotrimer and GPCR; however, this was attributed to constitutive activity of the GPCR constructs (26). We found that the addition of inverse agonists in our system did not abolish the FRET signal. In addition, it should be noted that basal currents measured in Fig. 1*C* were not increased from our previous studies (14), and we were able to demonstrate significant agonist-mediated increases in current.

It is quite plausible that there may be differences in precoupling between individual GPCRs and particular G proteins. Our data

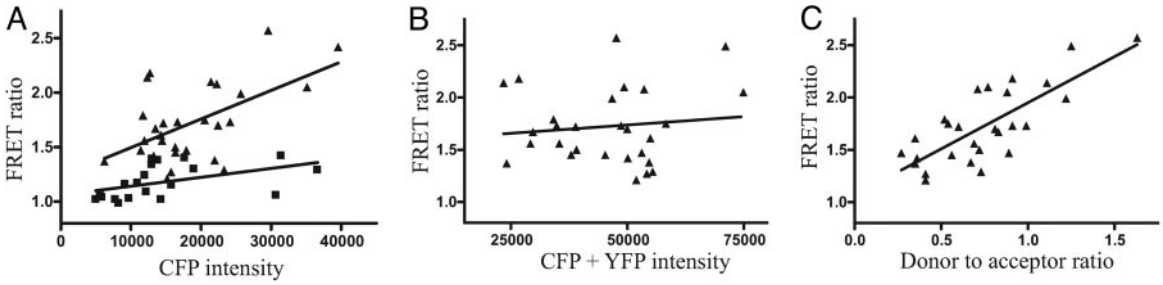

Fig. 6. Quantitative analysis of FRET. (*A*) FRET ratio is plotted against donor intensity/pixel for α2A-YFP+Go-CFP (inverted triangles) and α2A-YFP+Gs-CFP (squares). (*B* and *C*) The FRET ratio is independent of the donor plus acceptor intensity/pixel ($r^2 = 0.013$, not significant, *B*) but is strongly correlated with donor/acceptor ratio ($r^2 = 0.593$, $P < 0.0001$, *C*). The lines indicate the best-fit regression lines.

suggest such a possibility because the measured FRET ratio is greater with α2A-YFP and M4-YFP compared to D2-YFP ($P < 0.01$, ANOVA with Bonferroni post hoc test) and A1-YFP ($P < 0.01$, ANOVA with Bonferroni post hoc test). However, we would be cautious in interpreting the data in this fashion as the FRET ratio is sensitive to the donor/acceptor ratio and it would be necessary to perform a more detailed analysis before this could be established definitively. Such variations in precoupling may have functional consequences, as we have previously described differences in activation rates between different receptor families studied with saturating doses of agonist (13). Nevertheless, this could also be accounted for by differences in the properties of the different active ternary complexes. The addition of agonist led to a decrease in the FRET signal between Go-CFP and α2A-YFP, and this is consistent with models in which the active ternary complex is transitory in nature and the precoupled state is more stable. However, a number of other interpretations are possible, and changes in FRET ratio may be better examined by using photometry on the entire cell. Our method of analysis is complicated by movement of the cell membrane over time and the intrinsic noise associated with spatially resolved microscopy techniques.

Our current expression and microscopy conditions have been optimized to ensure roughly equivalent molar expression of the two proteins at moderate expression levels; this was determined by using a CFP–YFP dimer in which the ratio is physically constrained to 1:1. Interestingly, the FRET ratio varied between α2A-YFP and Go-CFP and was strongly dependent on the donor/acceptor ratio but not the absolute expression level. Thus, at 1:1 stoichiometries, it seems a proportion of the receptor and G protein pools are not associated. However, as the ratio of G protein to receptor increases, so does the degree of precoupling. Extrapolating to more physiological ratios, it seems likely that, where G protein is in significant excess compared to receptor, a large majority of receptor will be precoupled to G protein, but the majority of G proteins may not be coupled to receptor.

What are the advantages of such an arrangement? We originally investigated such issues to explain what factors contribute to the rapid activation of GIRK channels by Gi/o coupled receptors. In addition, we had previously found that the activation rate through a receptor–G protein fusion was identical to that of the normal receptor and increasing G protein concentration did not affect signaling kinetics (12). GPCR G protein precoupling can contribute to fast activation rates and can explain our previous experimental observations. Secondly, these interactions confer some selectivity to the signaling process. Such precoupling also does not preclude subsequent collision coupling, allowing signal amplification. We can now build up a picture of the receptor–G protein–GIRK signaling complex. In the basal state, the receptor, Gi/o heterotrimer, and channel are scaffolded together (14–17) and, on the addition of agonist, the complex may dissociate, allowing the receptor and perhaps the G protein α subunit to participate in other signaling processes. G$\beta\gamma$ may move from one domain of the channel to another, but it remains associated with the channel. Once again, our studies illustrate that the central role that the G protein α subunit has in orchestrating the GIRK channel signaling complex.

We are grateful to Dr. S Ikeda (National Institutes of Health, Bethesda) for providing cDNAs for Gβ1-YFP and Gγ2-CFP. This work was supported by the Wellcome Trust and the British Heart Foundation.

1. Tolkovsky, A. M. & Levitzki, A. (1978) *Biochemistry* **17,** 3795.
2. Gilman, A. G. (1987) *Annu. Rev. Biochem.* **56,** 615–649.
3. Hille, B. (1992) *Neuron* **9,** 187–195.
4. Tsunoda, S., Sierralta, J., Sun, Y., Bodner, R., Suzuki, E., Becker, A., Socolich, M. & Zuker, C. S. (1997) *Nature* **388,** 243–249.
5. Noma, A. & Trautwein, W. (1978) *Pflügers Arch.* **377,** 193–200.
6. Wickman, K., Nemec, J., Gendler, S. J. & Clapham, D. E. (1998) *Neuron* **20,** 103–114.
7. Drici, M. D., Diochot, S., Terrenoire, C., Romey, G. & Lazdunski, M. (2000) *Br. J. Pharmacol.* **131,** 569–577.
8. Yamada, M., Inanobe, A. & Kurachi, Y. (1998) *Pharmacol. Rev.* **50,** 723–757.
9. Logothetis, D. E., Kurachi, Y., Galper, J., Neer, E. J. & Clapham, D. E. (1987) *Nature* **325,** 321–326.
10. Reuveny, E., Slesinger, P. A., Inglese, J., Morales, J. M., Iniguez Lluhi, J. A., Lefkowitz, R. J., Bourne, H. R., Jan, Y. N. & Jan, L. Y. (1994) *Nature* **370,** 143–146.
11. Sodickson, D. L. & Bean, B. P. (1996) *J. Neurosci.* **16,** 6374–6385.
12. Benians, A., Leaney, J. L., Milligan, G. & Tinker, A. (2003) *J. Biol. Chem.* **278,** 10851–10858.
13. Benians, A., Nobles, M., Hosny, S. & Tinker, A. (2005) *J. Biol. Chem.* **280,** 13383–13394.
14. Leaney, J. L., Milligan, G. & Tinker, A. (2000) *J. Biol. Chem.* **275,** 921–929.
15. Leaney, J. L. & Tinker, A. (2000) *Proc. Natl. Acad. Sci. USA* **97,** 5651–5656.
16. Huang, C. L., Slesinger, P. A., Casey, P. J., Jan, Y. N. & Jan, L. Y. (1995) *Neuron* **15,** 1133–1143.
17. Peleg, S., Varon, D., Ivanina, T., Dessauer, C. W. & Dascal, N. (2002) *Neuron* **33,** 87–99.
18. Anger, S., Salahpour, A. & Bouvier, M. (2002) *Annu. Rev. Pharmacol. Toxicol.* **42,** 409–435.
19. Milligan, G. (2004) *Mol. Pharmacol.* **66,** 1–7.
20. Terrillon, S. & Bouvier, M. (2004) *EMBO Rep.* **5,** 30–34.
21. Munshi, R., Pang, I. H., Sternweis, P. C. & Linden, J. (1991) *J. Biol. Chem.* **266,** 22285–22289.
22. Freissmuth, M., Selzer, E. & Schutz, W. (1991) *Biochem. J.* **275,** 651–656.
23. Neubig, R. R., Gantzos, R. D. & Thomsen, W. J. (1988) *Biochemistry* **27,** 2374–2384.
24. Tian, W. N., Duzic, E., Lanier, S. M. & Deth, R. C. (1994) *Mol. Pharmacol.* **45,** 524–531.
25. Lachance, M., Ethier, N., Wolbring, G., Schnetkamp, P. P. & Hebert, T. E. (1999) *Cell Signal.* **11,** 523–533.
26. Gales, C., Rebois, R. V., Hogue, M., Trieu, P., Breit, A., Hebert, T. E. & Bouvier, M. (2005) *Nat. Methods* **2,** 177–184.
27. Baneres, J. L. & Parello, J. (2003) *J. Mol. Biol.* **329,** 815–829.
28. Ruiz-Velasco, V. & Ikeda, S. R. (2001) *J. Physiol.* **537,** 679–692.
29. Leaney, J. L., Benians, A., Graves, F. M. & Tinker, A. (2002) *J. Biol. Chem.* **277,** 28803–28809.
30. Benians, A., Leaney, J. L. & Tinker, A. (2003) *Proc. Natl. Acad. Sci. USA* **100,** 6239–6244.
31. Xia, Z. & Liu, Y. (2001) *Biophys. J.* **81,** 2395–2402.
32. Erickson, M. G., Alseikhan, B. A., Peterson, B. Z. & Yue, D. T. (2001) *Neuron* **31,** 973–985.
33. Benians, A., Nobles, M. & Tinker, A. (2004) *Biochem. Soc. Trans.* **32,** 1045–1047.
34. Takida, S. & Wedegaertner, P. B. (2003) *J. Biol. Chem.* **278,** 17284–17290.
35. Kenworthy, A. K., Petranova, N. & Edidin, M. (2000) *Mol. Biol. Cell* **11,** 1645–1655.
36. Pentcheva, T. & Edidin, M. (2001) *J. Immunol.* **166,** 6625–6632.
37. Erickson, M. G., Moon, D. L. & Yue, D. T. (2003) *Biophys. J.* **85,** 599–611.
38. Shryock, J. C., Ozeck, M. J. & Belardinelli, L. (1998) *Mol. Pharmacol.* **53,** 886–893.
39. Jansson, C. C., Kukkonen, J. P., Nasman, J., Huifang, G., Wurster, S., Virtanen, R., Savola, J. M., Cockcroft, V. & Akerman, K. E. (1998) *Mol. Pharmacol.* **53,** 963–968.
40. Hamm, H. E. (2001) *Proc. Natl. Acad. Sci. USA* **98,** 4819–4821.
41. Alousi, A. A., Jasper, J. R., Insel, P. A. & Motulsky, H. J. (1991) *FASEB J.* **5,** 2300–2303.
42. Ransnas, L. A. & Insel, P. A. (1988) *J. Biol. Chem.* **263,** 17239–17242.
43. Chabre, M. & Deterre, P. (1989) *Eur. J. Biochem.* **179,** 255–266.
44. Neubig, R. R. (1994) *FASEB J.* **8,** 939–946.
45. Kenakin, T. (1997) *Trends Pharmacol. Sci.* **18,** 456–464.
46. Law, S. F. & Reisine, T. (1997) *J. Pharmacol. Exp. Ther.* **281,** 1476–1486.
47. Kenakin, T. (2002) *Annu. Rev. Pharmacol. Toxicol.* **42,** 349–379.